sustainability

MDPI

Article

Pi-pi Stacking-Driven Nucleation of Aromatic Oxygenated Organic Molecules: Implications for Sustainable Urban Air-Quality Management

Yiran Deng, Yongjun Han, Xinyu Liu, Yaxin Li, Haojie Xu, Hu Zhao and Xiangli Shi *

College of Geography and Environment, Shandong Normal University, Jinan 250014, China; 2025215101@stu.sdnu.edu.cn (Y.D.); 202414500115@stu.sdnu.edu.cn (Y.H.); 202414500116@stu.sdnu.edu.cn (X.L.); 202414500106@stu.sdnu.edu.cn (Y.L.); 2023026906@stu.sdnu.edu.cn (H.X.); 2023026921@stu.sdnu.edu.cn (H.Z.)
* Correspondence: shixl@sdnu.edu.cn

Abstract

Aromatic compounds are abundant in urban and industrial environments and potentially serve as one of the primary precursors for new particle formation (NPF). Pi-pi stacking is a distinctive weak interaction observed between aromatic compounds. Aromatic oxygenated organic molecules (AOOM) are key products of atmospheric oxidation of aromatic compounds; however, the role of pi-pi stacking in their involvement in atmospheric new particle formation (NPF) remains unclear. This study used quantum chemical calculations to reveal the nucleation mechanism of AOOM through pi-pi stacking and hydrogen bonding. The results indicate that the contribution of pi-pi stacking to nucleation in aromatic compounds is primarily determined by the stacking area. For aromatic hydrocarbons with 1–2 phenyl groups, the Gibbs free energy (ΔG) of dimolecular clusters formed solely by pi-pi stacking is positive. In contrast, for polycyclic aromatic hydrocarbons with three or more phenyl groups, the ΔG of these clusters decreases significantly and becomes negative. Single-phenyl AOOM primarily participates in the NPF process through hydrogen bonding with sulfuric acid molecules. In this work, an explanation is provided for observations and laboratory findings of the appearance of aromatic-ring-retaining species in nanoparticles. The discovery of pi-pi stacking also completes the variety of atmospheric nucleation weak interactions. The oxidation and nucleation mechanisms of aromatic compounds should be reassessed, considering the effects of pi-pi stacking, especially polycyclic aromatic hydrocarbons. These findings have important implications for sustainable urban air-quality management. By clarifying the role of pi-pi stacking, particularly in polycyclic aromatic hydrocarbons, this study may improve predictions of new particle formation, refine secondary organic aerosol modeling, and inform targeted emission-control policies to protect public health and mitigate climate impacts.

Keywords: pi-pi stacking; new particle formation; aromatic compounds; oxygenated organic molecules; nucleation mechanism; urban aerosol sustainability

Check for updates

Academic Editor: Rafal Przekop

Received: 26 April 2026
Revised: 21 May 2026
Accepted: 21 May 2026
Published: 27 May 2026

Copyright: © 2026 by the authors. Licensee MDPI, Basel, Switzerland. This article is an open access article distributed under the terms and conditions of the Creative Commons Attribution (CC BY) license.

1. Introduction

New particle formation (NPF) events are frequently observed in densely populated areas, such as cities and industrial zones, and strongly impact the formation of atmospheric aerosols, air quality, and public health [1–9]. New particle formation proceeds by nucleation and growth, where sulfuric acid (SA) is recognized as a crucial precursor for the nucleation process [10–12]. Oxygenated organic molecules (OOMs) are considered to be

effectively nonvolatile and, in conjunction with SA, contribute to the nucleation and growth of new particle formation [13,14]. Highly oxygenated organic molecules (HOMs), a type of OOMs, typically contain multifunctional groups. HOMs with extremely low volatilities can irreversibly condense on nanoparticles [14–17]. However, there is no direct evidence of OOM participation in the initial nucleation stage [18].

Oxidation reactions initiated by OH radicals, O_3, and NO_3 radicals in the atmosphere rapidly transform volatile organic compounds (VOCs) into abundant quantities of OOMs [19–21]. These OOMs and other stabilizers (e.g., SA, nitric acid (NA), bases and ions) form stable clusters through weak interactions, promoting NPF [22,23]. The various organic functional groups in OOMs, such as carboxyl, peroxide and hydroxyl, act as donors/acceptors as well as bridges for cluster stabilization [19]. Previous theoretical studies on weak interactions among atmospheric OOM clusters have primarily focused on electrostatic interactions, including hydrogen bonding, proton transfer, and halogen bonding [24–28]. This emphasis results from electrostatic interactions typically prevailing over van der Waals forces between polar (or locally polar) OOMs and other molecules involved in the formation of clusters. Thus, the role of van der Waals forces in cluster formation has been neglected.

Nie et al. [29] found that the oxidation of anthropogenic VOCs was the primary source of OOMs in major cities across China, including Beijing, Shanghai, Nanjing, and Hong Kong. The formation of approximately 40% of OOMs was attributed to the oxidation of aromatic compounds. Aromatic hydrocarbons, through atmospheric oxidation, can produce both open-ring OOMs and aromatic ring-retaining OOMs [30]. Zheng et al. [22] observed that aromatic ring-retaining OOMs, collectively known as AOOM, comprised more than 6% of the total OOM concentration in ambient measurements conducted in South China. The pi-pi interaction is a distinctive feature of aromatic compounds. Aromatic compounds can aggregate not only through hydrogen bonds, electrostatic interactions, etc., but pi-pi stacking can also promote the condensation of clusters [31]. The more aromatic rings in the cluster molecules, the more pronounced the pi-pi stacking effect. When polycyclic aromatic hydrocarbons contain four rings, the binding energy of the resulting bimolecular cluster is approximately −17 kcal/mol [31]. Aromatic OOMs generally exhibit higher toxicity than open-ring OOMs, posing greater harm to human health when incorporated into particulate matter [32]. Abundant aromatic compounds in the atmosphere, such as alkylbenzenes, oxidized aromatic hydrocarbons, and polycyclic aromatic hydrocarbons, can undergo oxidation processes initiated by OH radicals to produce AOOM [33–35]. There is no clear understanding of the mechanism of oxidation of aromatic compounds in the atmosphere of cities and industrial areas to generate AOOM that participate in the nucleation and growth of new particles via pi-pi stacking.

The photooxidation of atmospheric VOCs produces a wide variety of OOMs with complex and trace structures [36–38]. It is extremely challenging to determine the exact functional groups and arrangement of OOMs and to distinguish the different roles they play in nucleation and growth. Quantum chemical calculations can be employed to investigate the mechanism of OOM formation from VOCs and assess the capacities of different given OOM structures to form clusters [39–42]. Common density functional theory (DFT) approaches include B3LYP, range-separated hybrid functionals such as ωB97X-D, and meta-hybrid functionals such as M06-2X. B3LYP is efficient for initial conformational searches, but it can underestimate dispersion forces that are critical for pi-pi stacking. ωB97X-D provides reliable geometries with moderate-cost dispersion correction, whereas M06-2X offers higher accuracy for non-covalent interactions in organic clusters, although it is computationally more demanding. These methods are widely used because they provide a practical balance between computational efficiency and reliability for systems containing up to ap-

proximately 50 atoms. However, they may still produce errors of 1–3 kcal/mol in binding energies and Gibbs free energies, especially for dispersion-dominated oxygenated organic molecules that retain aromatic rings. Wavefunction-based methods, especially DLPNO-CCSD(T)/aug-cc-pVTZ calculations or complete-basis-set extrapolation, are considered the current gold standard for final electronic energies. They provide benchmark-level accuracy for weak interactions while remaining computationally feasible when combined with DFT-optimized geometries [43,44]. The nucleation mechanism of AOOM produced by the oxidation of different aromatics via pi-pi stacking was investigated in this study. Thermodynamic and topological analyses were performed to determine the influence of functional groups on the benzene ring and branched chain on the nucleation of AOOM. The effects of NA on the formation of AOOM clusters were investigated. Our studies of pi-pi stacking have contributed to elucidating the weak interaction mechanism of organic vapors involved in atmospheric nucleation and growth.

2. Methods

2.1. Quantum Chemical Calculations

The initial geometries of clusters and molecules were generated by the basin-hopping Monte Carlo method. The AMPAC program was then used to perform simulated annealing for further generation of clusters and molecules. The resulting rational configurations were optimized at the B3LYP/6-31g(d,p) level. The simulated annealing and DFT calculations were iterated until the conformer with the lowest energy between iterations reached a single-point energy below 2 kcal/mol. In these iterative calculations, all the lowest energy configurations within a 5 kcal/mol range were optimized at the more accurate M06-2X/6-31+G(d,p) level, and their corresponding harmonic vibrational frequencies were calculated at the same level. All calculations using the B3LYP and M06-2X methods were performed at 298 K and 1 atm. The corresponding single-point energies were further computed at the DLPNO-CCSD(T)/aug-cc-pVTZ level using the ORCA program (4.2.1 Version) [45]. The M06-2X/6-31+G(d,p)//DLPNO-CCSD(T)/aug-cc-pVTZ method excels in accurately predicting weak intermolecular interactions in organic systems [27,46]. All the DFT calculations were carried out using the Gaussian 16 program (Revision A.03) in a vacuum environment [47]. The lowest energy configurations and Cartesian coordinates of all the clusters and molecules are shown in Figures S1 and S2 and Table S4, respectively.

The binding energy of the system is determined by computing the electronic energy difference between the system and its constituent monomers, employing the Counterpoise Correction method to mitigate the basis set superposition error (BSSE), otherwise resulting in a lower total energy of the system calculated and an overestimation of the interaction energy due to the overlap of basis functions, causing the basis set used in the calculation to be larger than that used in the individual calculation [48]. The Gibbs free energy of the cluster is derived from the energy difference between the reactants and products, with thermodynamic corrections, including vibrational frequency analysis, applied to precisely capture temperature-dependent effects.

2.2. IRI Analysis

The weak interactions of clusters were analyzed using the interaction region indicator (*IRI*) function [48], which is defined as

$$IRI(\boldsymbol{r}) = \frac{|\nabla\rho(\boldsymbol{r})|}{[\rho(\boldsymbol{r})]^a} \quad (1)$$

where ρ is the electron density and a is an adjustable parameter (usually set to 1.1). The sign(λ_2)ρ function is used to determine the strength and character of the interactions in the

different regions by projecting onto *IRI* isosurfaces in different colours. Green represents weak interactions, red indicates strong site resistance, and blue indicates very strong weak interactions, such as hydrogen bonding (Figure 1).

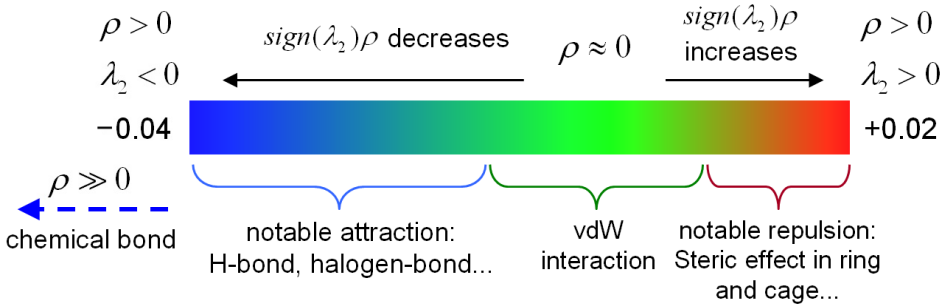


Figure 1. Standard coloring scheme and corresponding chemical interpretation of the sign(λ_2)ρ function on the *IRI* isosurface. On the *IRI* isosurfaces, regions with van der Waals interactions are shown in green, regions with sites offering spatial resistance are shown in red, regions with low-level weak interactions are shown in light blue, and regions with strong weak interactions or chemical bonding are shown in blue. The arrows in the picture indicate the changes in the direction trend as indicated by the arrows.

3. Results and Discussion

3.1. The Importance of Pi-pi Stacking

To evaluate the role of pi-pi stacking in atmospheric nucleation processes, this study first analyzed the weak interactions and thermodynamic properties of $(benzene)_2$, $(naphthalene)_2$, $(anthracene)_2$, and $(phenanthrene)_2$ dimolecular clusters. As shown in Figure 2, pi-pi stacking is present in the dimolecular clusters of these aromatic hydrocarbons, with the green areas indicating the regions of pi-pi stacking. As the number of aromatic rings increases, the interaction area of the pi-pi stacking increases significantly. The binding energies of $(benzene)_2$, $(naphthalene)_2$, $(anthracene)_2$, and $(phenanthrene)_2$ clusters are −3.05, −7.29, −11.82, and −11.76 kcal/mol, respectively (Table S1). Further analysis of the temperature effects on cluster formation reveals that Gibbs free energy for cluster formation (ΔG) for the $(benzene)_2$, $(naphthalene)_2$, $(anthracene)_2$, and $(phenanthrene)_2$ clusters are 3.92, 0.24, −5.11, and −1.53 kcal/mol at 298 K, respectively. This suggests that the stabilizing effect of pi-pi stacking on the formation of clusters in $(benzene)_2$, $(naphthalene)_2$ clusters is minimal. A strong stabilizing effect is observed only when the pi-pi stacking interaction area is sufficiently large, such as in the $(anthracene)_2$ cluster.

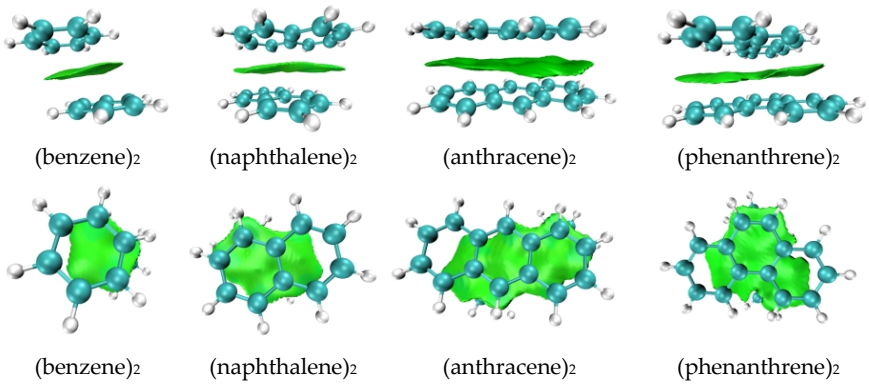


Figure 2. Interaction region indicator (*IRI*) analysis of $(benzene)_2$, $(naphthalene)_2$, $(anthracene)_2$, and $(phenanthrene)_2$ clusters. Van der Waals forces are indicated in green, strong attraction (such as covalent and hydrogen bonding) is indicated in blue, and strong repulsion (such as steric hindrance) is indicated in red.

3.2. Effects of Functional Groups on the Branched Chain

Subsequently, we investigated how different functional groups on the oxidized branched chain of the benzene ring affect the nucleation of AOOM. The compounds A, E, G1, G2, H, and I are produced by direct emissions or the atmospheric oxidation of aromatic compounds, and B, C, D, and F are compounds that we designed to study the effect of functional groups on the nucleation of AOOM (Table 1). The largest difference among the volatilities of these AOOM was approximately seven orders of magnitude.

Table 1. Molecular structure, O/C ratio and saturated vapor pressure of A, B, C, D, E, F, G1, G2, H and I.

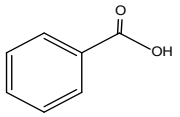
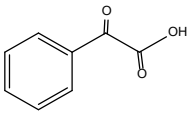
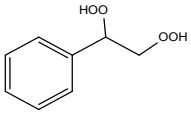
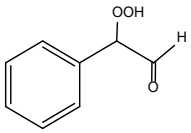
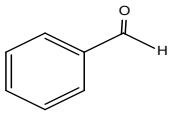
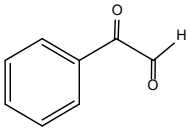
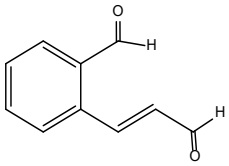
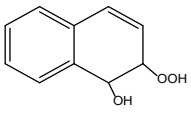
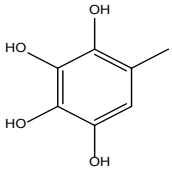
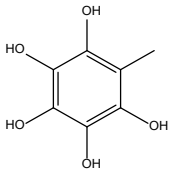
	Molecule Structure	Source	O/C Ratio	Saturated Vapor Pressure
A (benzoic acid)		Direct emission, benzaldehyde oxidation [33,49] (SI Figure S3a)	2/7	$p = 5.05 \times 10^{-4}$
B			3/8	$p = 2.21 \times 10^{-5}$
C			4/8	$p = 8.58 \times 10^{-6}$
D			3/8	$p = 1.08 \times 10^{-4}$
E (benzaldehyde)		Direct emission [50]	1/7	$p = 7.85 \times 10^{-2}$
F			2/8	$p = 3.43 \times 10^{-3}$
G1		Naphthalene oxidation [35] (Figure S3b)	2/10	$p = 1.57 \times 10^{-4}$
G2		Naphthalene oxidation [35] (Figure S3b)	3/10	$p = 1.90 \times 10^{-6}$
H		Toluene oxidation [51] (Figure S3c)	4/7	$p = 3.06 \times 10^{-9}$

Table 1. *Cont.*

	Molecule Structure	Source	O/C Ratio	Saturated Vapor Pressure
I		Toluene oxidation [51] (Figure S3c)	5/7	$p = 1.97 \times 10^{-11}$

As shown in Table 2, it is challenging for these AOOM to independently form pure trimolecular organic clusters because of the high ΔG values $(AOOM)_3$. Therefore, it is imperative to consider the nucleation abilities of AOOM in the presence of SA molecules. For benzoic acid (Molecule A), a $(A)_2(SA)$ cluster can form in the presence of a single SA molecule. However, the addition of another A molecule to form a $(A)_3(SA)$ cluster only results in a ΔG of −0.65 kcal/mol. Thus, benzoic acid (in which there is only one carboxyl group on the benzene ring) has a relatively weak ability to nucleate and one SA molecule cannot adequately sustain cluster growth. The abundant benzoic acid in the atmosphere predominantly facilitates the growth of newly formed nanoparticles [1,49]. Calculations were also performed on the nucleation of phenylglyoxylic acid (B), which contains a carboxyl group and an acyl group. A similar trend was found for the nucleation of Molecule B to that of Molecule A in the presence of one SA molecule. Molecules C and G2 possess two and one hydroperoxy groups (–OOH), respectively, and can both undergo continuous condensation with a AOOM molecule via the formation of (AOOM)(SA) to thermodynamically form $(AOOM)_3(SA)$. The formation of $(AOOM)_3(SA)$ is more favorable for Molecule C than for G2. Despite not being a HOM and having fewer than 10 C atoms, Molecule C is semivolatile because of its relatively high saturated vapor pressure. The strong nucleation ability of Molecule C is attributed to the presence of one phenyl group and two –OOH groups.

Table 2. The Gibbs free energy of formation ΔG (kcal/mol) of clusters of A, B, C, D, E, F, G1, G2, H, and I compounds calculated at 298 K and 1 atm.

	Clusters	ΔG		Clusters	ΔG
A	$A + SA \rightleftarrows (A)(SA)$	−7.28	B	$B + SA \rightleftarrows (B)(SA)$	−6.76
	$A + A \rightleftarrows (A)_2$	−5.31		$B + B \rightleftarrows (B)_2$	−4.64
C	$C + SA \rightleftarrows (C)(SA)$	−10.60	G2	$G2 + SA \rightleftarrows (G2)(SA)$	−7.66
	$C + C \rightleftarrows (C)_2$	−9.11		$G2 + G2 \rightleftarrows (G2)_2$	−5.09
D	$D + SA \rightleftarrows (D)(SA)$	−4.87	F	$F + SA \rightleftarrows (F)(SA)$	−0.66
	$D + D \rightleftarrows (D)_2$	2.15		$F + F \rightleftarrows (F)_2$	1.13
E	$E + SA \rightleftarrows (E)(SA)$	−3.47	G1	$G1+SA \rightleftarrows (G1)(SA)$	−4.18
	$E + E \rightleftarrows (E)_2$	2.42		$G1+G1 \rightleftarrows (G1)_2$	−4.18
H	$H + SA \rightleftarrows (H)(SA)$	−3.95	I	$I + SA \rightleftarrows (I)(SA)$	−2.71
	$H + H \rightleftarrows (H)_2$	−0.46		$I + I \rightleftarrows (I)_2$	0.07

$\rightleftarrows$ denotes a reversible chemical reaction.

The four molecules D, F, E, and G1 all feature one or two aldehyde groups on the branched chain of the benzene ring. However, these molecules have a limited ability to form $(AOOM)_2$ or (AOOM)(SA). This result suggests that the presence of aldehyde groups on the branched chain of the benzene ring hinders AOOM nucleation. The nucleation capacity of each of these AOOM is directly correlated with its saturated vapor pressure. That is, a low saturated vapor pressure indicates a high propensity for nucleation. Molecules H

and I are polyhydroxy-substituted phenolic compounds that are also HOMs. None of the branched chains (i.e., the methyl groups) of Molecules H and I are oxidized. It is thermodynamically difficult for both Molecules H and I to form bimolecular clusters with SA or alone, indicating that the presence of oxidized aliphatic chains in AOOM is essential for participation in the initial stage of nucleation.

3.3. Substituents on the Benzene Ring

In addition to undergoing addition reactions with OH and Cl radicals in the atmosphere, aromatic hydrocarbon compounds can also undergo displacement of hydrogen atoms on aromatic rings to produce phenols and halogenated benzene [30,34,52]. These products may subsequently be oxidized to generate phenolic and chlorinated AOOM. Therefore, we also considered the effect of substituents on the benzene ring of AOOM on the nucleation of AOOM. The –Cl and –OH groups are electron-withdrawing and electron-donating, respectively. Taking Molecule B as an example, the formation of the (B1)(SA) cluster containing the chlorine-substituted molecule B1 is less thermodynamically favorable than the formation of (B)(SA), and the formation of $(B1)_2$ is less thermodynamically favorable than the formation of $(B)_2$ (Figure 3). Thus, the presence of electron-withdrawing groups, such as –Cl, on the benzene ring is not favorable for the nucleation of AOOM through hydrogen bonding and pi-pi stacking. Molecule B2 is a hydroxyl-substituted compound and a HOM. There is a higher propensity for the formation of both (B2)(SA) and $(B2)_2$ than the corresponding clusters containing B and B1. However, B2 has a weaker nucleation ability than Molecule C despite the ability to form $(B2)_3$(SA) through the pathway of $(B2)_2$ formation followed by $(B2)_2$(SA) formation (see Figure 3 and Table 2). A comparison of the configurations and ΔG values of the $(B)_2$ and $(B2)_2$ clusters (Figure S2 and Figure 3) shows that the multiple hydroxyl groups on the benzene ring of AOOM mainly provide additional sites for the formation of hydrogen bonds and have little effect on the strength of pi-pi stacking.

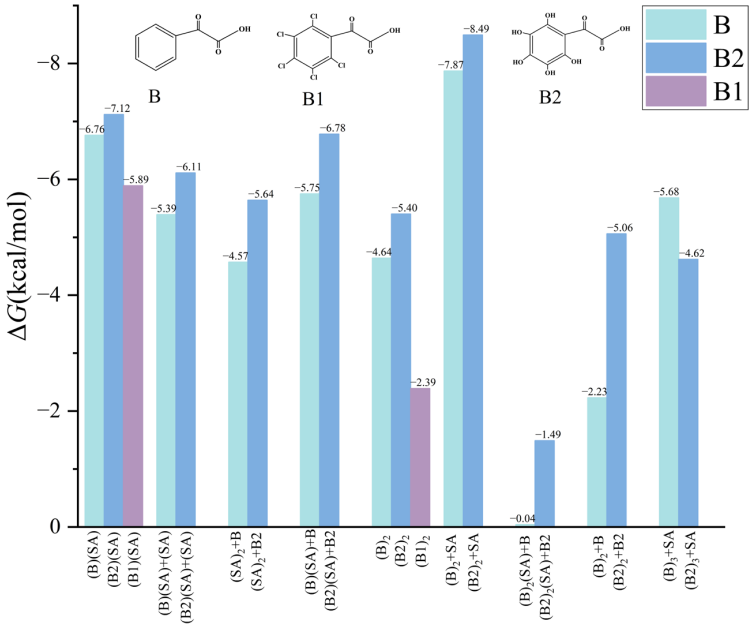


Figure 3. The Gibbs free energy of formation ΔG (kcal/mol) of clusters of B, B1, and B2, calculated at 298 K and 1 atm, are represented by green, purple, and blue bars, respectively.

3.4. Comparative Analysis of Nucleation Mechanisms

The importance of the role played by OOMs in aerosol growth is widely acknowledged, whereas it is uncertain whether OOMs also play an important role in aerosol nucleation in

the atmosphere [18]. A variety of atmospheric nucleation mechanisms have been reported, such as for SA–H_2O [53], SA–NH_3 [54], SA–amine [3], oxidized organic matter [55], and iodine oxides [25,56]. Field observation has confirmed the presence of SA–DMA in a polluted environment [57], where it plays a particularly important role in the initial stage of nucleation. Therefore, we compared the optimal nucleation pathways of three systems: SA–DMA, pure SA, and SA–AOOM. We employed thermodynamic data to determine the magnitude of the growth of clusters in each system. The lowest energy configurations of the $(SA)_{1–4}(DMA)_{1–4}$ clusters were obtained from the study by Myllys et al. [58]. Here, we recalculated their vibrational frequencies and single-point energies using the M06-2X/6-31+G(d,p)//DLPNO-CCSD(T)/aug-cc-pVTZ method. The ΔG values of all the clusters of $(SA)_{1–4}(DMA)_{1–4}$ are shown in Table S2.

Among the aforementioned AOOM, C has the highest propensity to nucleate in the presence of one SA molecule and can both form a critical nucleus. Specifically, $(C)_3(SA)$ has a nuclear diameter of 1.2 nm. A comparison of the ΔG values of three systems (SA–DMA, SA–C, and pure SA, Figure 4) reveals that the thermodynamic difficulty of forming bimolecular and trimolecular clusters increases in the order of SA–DMA, SA–C, and pure SA. It is considerably easier for SA–DMA to form clusters than the other two systems. The largest $(SA)_4(DMA)_4$ cluster was calculated to have a diameter of approximately 1.3 nm. There is a small difference in the difficulty of forming tetrameric clusters among the three systems. The formation of $(SA)_2(DMA)_2$ is the most feasible, followed by the formation of $(SA)_4$, and $(C)_3(SA)$. Although DMA has a strong stabilizing effect on SA, $(SA)_4(DMA)_4$ formation requires the participation of multiple SA molecules. Similarly, Molecule C can form clusters larger than 1 nm in diameter via hydrogen bonds in the presence of one SA molecule. The ΔG for the formation of the $(C)_3(SA)$ cluster, resulting from the addition of one more C molecule to the $(C)_2(SA)$ cluster, is only −3.65 kcal/mol. This suggests that a single SA molecule is insufficient to maintain the continuous growth of the SA–C clusters. Nitric acid plays an important role in promoting the formation of new particle clusters [57]. In this study, we investigated the nucleation mechanism of the binary system NA–AOOM (Table S3). Nitric acid has a considerably weaker stabilizing effect on AOOM than SA, resulting in thermodynamically unstable NA–AOOM clusters.

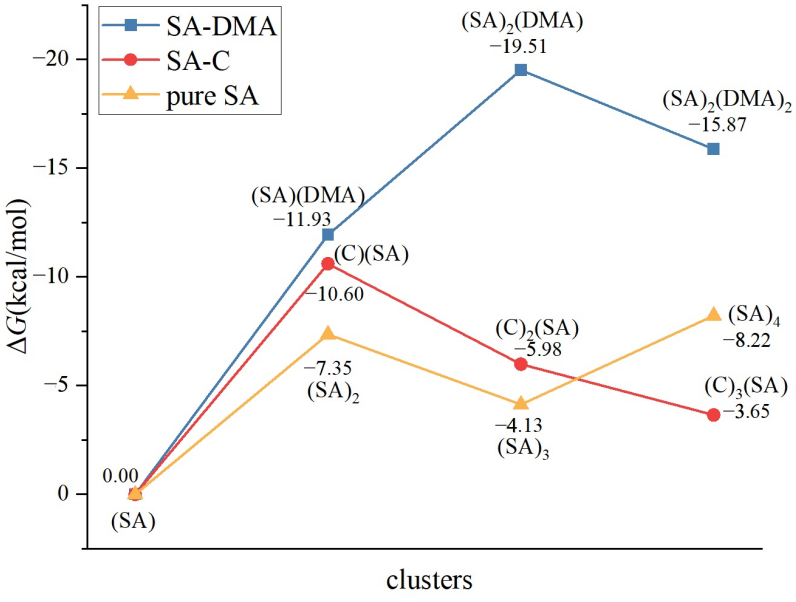


Figure 4. Gibbs free energy of formation ΔG (kcal/mol) of pure sulfuric acid (SA), SA–DMA (DMA = dimethylamine), and SA–AOOM (AOOM = C) calculated at the at 298 K and 1 atm. The blue, yellow, and red folded lines correspond to the SA–DMA, pure SA, and SA–C systems, respectively.

4. Atmospheric Implications

The dominant mechanism of removal of aromatic compounds from the atmosphere is reaction with OH radicals (Figure 5) [59,60]. This reaction mainly proceeds by OH addition to the benzene ring and abstraction of a H atom from the branched chain [37,61]. The OH radical preferentially undergoes addition reactions on the branched chain when the chain contains unsaturated double bonds, e.g., styrene [62]. These reactions of the aromatic ring produce adducts that then react with O_2 to form phenolic compounds (Pathway 1) and bicyclic peroxy radicals (BPRs, Pathway 2). These intermediates serve as precursors for conventional autoxidation and phenolic pathways, respectively, contributing to the formation of multifunctional HOMs. The branched chains of aromatic compounds can also be susceptible to attack by OH radicals, leading to H-abstraction or OH-addition reactions. The formation of RO_2 radicals through addition to O_2 ultimately leads to the generation of AOOM via radical termination reactions (Pathways 3 and 4). The importance of the atmospheric nucleation of AOOM produced by Pathways 3 and 4 has not been recognized in the literature. In addition to monocyclic aromatic compounds in the atmosphere, polycyclic aromatic hydrocarbons (e.g., naphthalenes, biphenyls, indoles, and quinolines) can generate AOOM through ring scission initiated by the attack of OH radicals on one of their aromatic rings [35,63–65].

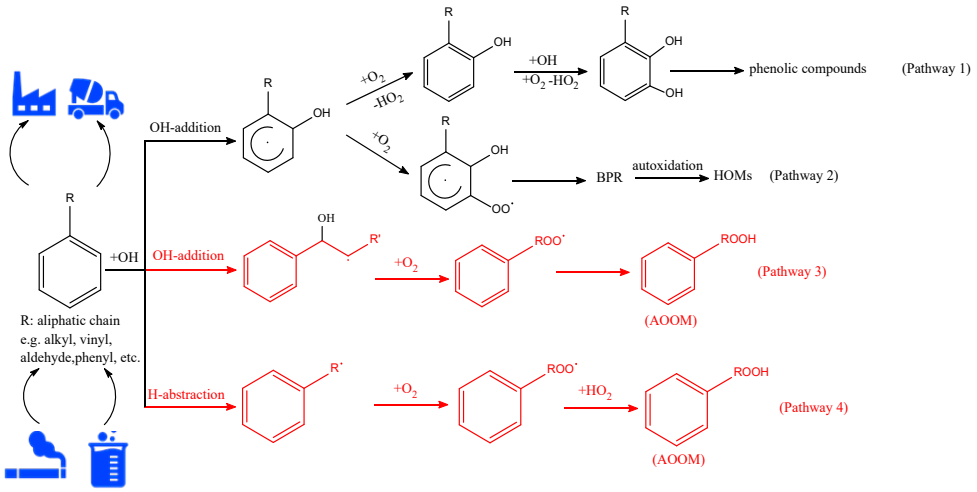


Figure 5. Several common reaction pathways for aromatic compounds in the atmosphere.

The aromatic-ring-opening HOM monomers generated through Pathway 2 contain multifunctional groups that typically enable cluster formation solely via hydrogen bonding with nucleation precursors, such as SA molecules [16,36,66]. These volatile HOM monomers are thought to mainly participate in the growth phase, whereas the extremely volatile HOM dimers are hypothesized to participate in the initial nucleation stage [67,68]. The yield of HOMs from aromatic oxidation is often below 3% [69]. In an environment with a high concentration of OH radicals, aromatic hydrocarbons undergo oxidation by multiple generations of OH radicals to form phenolic compounds via Pathway 1. However, despite being HOMs, these phenolic compounds are much less able to participate directly in nucleation than AOOM (Table 2). An analysis of the results of chamber and flow experiments [37,70] revealed that the presence of a large number of aromatic-ring-retaining OOMs in the particle phase, in addition to aromatic-ring-opening HOMs. In South China, some ring-retaining OOMs (6%) were also detected in the atmospheric particle phase by ambient measurement [22]. According to this study, these ring-retaining OOMs are likely to be AOOM, which can participate in the formation of nanoparticles through hydrogen bonding.

Yin et al. [71] characterized neutral clusters of pure SA during NPF in urban Beijing. Our theoretical calculations show that the likelihood of AOOM with –OOH groups on the branched chain form clusters with one SA molecule is sufficient to compete with the nucleation of pure SA (Figure 4). However, AOOM have a weaker stabilizing effect on SA than DMA. The SA–DMA nucleation mechanism alone does not fully explain the observed NPF rates [71–74]. Cai et al. [12] reported the presence of a substantial number of unidentified species, in addition to SA and DMA, during NPF in Beijing. Both HOMs and AOOM are candidates for these unidentified species. We found that AOOM with –OOH groups on the branched chain need SA molecules to form clusters at the critical nuclei scale. Therefore, in environments in which the oxidation of aromatic compounds produces a substantial abundance of AOOM, NPF events may also be initiated at relatively high SA concentrations. By contrast, NA has a considerably weaker tendency to nucleate with AOOM than SA.

5. Conclusions

This study used quantum chemical calculations to examine the role of pi-pi stacking interactions in the initial nucleation of new particle formation. The results show that clusters formed through pi-pi stacking in aromatic compounds with one or two benzene rings are thermodynamically unstable. In polycyclic compounds with three or more benzene rings, cluster stability is significantly enhanced and positively correlates with the pi-pi stacking contact area. For AOOMs with only one aromatic ring, their participation in early nucleation requires SA molecules to stabilize the cluster. The -OOH group on the branched chain of AOOM facilitates hydrogen bonding with SA, promoting SA-organic cluster nucleation. Substituents on the benzene ring, such as OH and Cl, exert minimal influence on AOOM nucleation.

Typically, AOOM are formed through the oxidation of aromatic compounds by first-generation OH radicals and may subsequently be further oxidized by second or subsequent-generation OH radicals in the atmosphere to form HOM monomers. The entry of oxygenated organic molecules with various molecular structures into atmospheric particles produces widely differing effects on humans. Hence, AOOM and ring-opening HOMs do not only differ in terms of their roles in the atmospheric nucleation mechanism but also in their impacts on human health. It is imperative to better identify atmospheric AOOM to comprehensively understand their nucleation and growth mechanisms, as well as their impacts on the environment and humans. The insights from this study directly inform sustainable development goals by underscoring the importance of multigenerational oxidation pathways of aromatic VOCs in urban environments. Integrating AOOM monitoring into existing air-quality networks and accounting for pi-pi stacking in chemical transport models will improve the evaluation of secondary organic aerosol formation, population exposure risks, and the effectiveness of air-pollution control policies—critical steps toward healthier and more sustainable cities.

Supplementary Materials: The following supporting information can be downloaded at https://www.mdpi.com/article/10.3390/su18115375/s1: Figure S1: Lowest energy configurations of A to I calculated at the M06-2X/6-31+G(d,p) level. Oxygen-carbon ratios and vapor pressures are labelled in the graphs; Figure S2: The lowest energy configurations of all clusters optimized at the M06-2X/6-31+G(d,p) level; Figure S3a: Benzoic acid formed by oxidation of benzaldehyde; Figure S3b: Atmospheric oxidation of G1 and G2 compounds by naphthalene; Figure S3c: Atmospheric oxidation of compounds H and I by toluene; Table S1: Gibbs free energy of formation (ΔG, kcal/mol) and binding energy (ΔE, kcal/mol) of $(benzene)_2$, $(naphthalene)_2$, $(anthracene)_2$, and $(phenanthrene)_2$ clusters; Table S2: Gibbs free energy of formation ΔG (kcal/mol) of clusters of SA and DMA; Table S3: Gibbs free energy of formation ΔG (kcal/mol) of clusters of C compounds with NA calculated at 298 K and 1 atm; Table S4: Cartesian coordinates of molecules and clusters.

Author Contributions: Conceptualization, Y.D.; methodology, Y.H.; software, H.X.; validation, Y.D., Y.H. and X.L.; formal analysis, Y.L.; investigation, H.X.; resources, X.S.; data curation, H.Z.; writing—original draft preparation, Y.D.; writing—review and editing, X.S.; visualization, Y.D.; supervision, H.X.; project administration, X.S.; funding acquisition, X.S. All authors have read and agreed to the published version of the manuscript.

Funding: This research was funded by the National Natural Science Foundation of China (Grant No. 22276114).

Institutional Review Board Statement: Not applicable.

Informed Consent Statement: Not applicable.

Data Availability Statement: The original contributions presented in this study are included in the article/Supplementary Material. Further inquiries can be directed to the corresponding author.

Conflicts of Interest: The authors declare no conflicts of interest.

References

1. Zhang, R.; Suh, I.; Zhao, J.; Zhang, D.; Fortner, E.C.; Tie, X.; Molina, L.T.; Molina, M.J. Atmospheric new particle formation enhanced by organic acids. *Science* **2004**, *304*, 1487–1490. [CrossRef] [PubMed]
2. Kulmala, M.; Vehkamäki, H.; Petäjä, T.; Dal Maso, M.; Lauri, A.; Kerminen, V.M.; Birmili, W.; McMurry, P.H. Formation and growth rates of ultrafine atmospheric particles: A review of observations. *J. Aerosol Sci.* **2004**, *35*, 143–176. [CrossRef]
3. Yao, L.; Garmash, O.; Bianchi, F.; Zheng, J.; Yan, C.; Kontkanen, J.; Junninen, H.; Mazon, S.B.; Ehn, M.; Paasonen, P.; et al. Atmospheric new particle formation from sulfuric acid and amines in a Chinese megacity. *Science* **2018**, *361*, 278–281. [CrossRef]
4. Chukwu, T.M.; Morse, S.; Murphy, R. Poor air quality in urban settings: A comparison of perceptual indicators, causes and management in two cities. *Sustainability* **2022**, *14*, 1438. [CrossRef]
5. Agibayeva, A.; Guney, M.; Karaca, F.; Kumisbek, A.; Kim, J.R.; Avcu, E. Analytical methods for physicochemical characterization and toxicity assessment of atmospheric particulate matter: A review. *Sustainability* **2022**, *14*, 13481. [CrossRef]
6. Kang, B.; Liu, C.; Miao, C.; Zhang, T.; Li, Z.; Hou, C.; Li, H.; Li, C.; Zheng, Y.; Che, H. A comprehensive study of a winter haze episode over the area around bohai bay in northeast China: Insights from meteorological elements observations of boundary layer. *Sustainability* **2022**, *14*, 5424. [CrossRef]
7. Chen, Y.; Lin, H.; Wang, J.; Li, F.; Amouri, R.E.L.; Ip, J.C.-H.; Liu, W.; Mo, J. Multigenerational developmental and skeletal toxicity from benzo[a]pyrene exposure in F0 and F2 medaka: Metabolic trade-offs and survival costs. *New Contam.* **2026**, *2*, e002. [CrossRef]
8. Liu, Z.; Liu, Y.; Zhang, H.; Zhao, Y.; Zhang, T.; Cai, Y.; Xue, J. A brief review of strobilurin fungicides: Environmental exposure, transformation, and toxicity. *New Contam.* **2025**, *1*, e004. [CrossRef]
9. Chen, C.; Zhang, H.; Sun, Y.; Li, J.; Zhang, Z.; Gao, J.; Gao, R.; Wei, L.; Ma, N.; Xu, W.; et al. Characterization and influencing factors of hydroxymethanesulfonate (HMS) in the north China plain: Integration of field measurements and theoretical calculations. *Atmos. Environ.* **2026**, *367*, 121731. [CrossRef]
10. Lin, Y.; Ji, Y.; Li, Y.; Secrest, J.; Xu, W.; Xu, F.; Wang, Y.; An, T.; Zhang, R. Interaction between succinic acid and sulfuric acid–base clusters. *Atmos. Chem. Phys.* **2019**, *19*, 8003–8019. [CrossRef]
11. Kirkby, J.; Curtius, J.; Almeida, J.; Dunne, E.; Duplissy, J.; Ehrhart, S.; Franchin, A.; Gagné, S.; Ickes, L.; Kürten, A.; et al. Role of sulphuric acid, ammonia and galactic cosmic rays in atmospheric aerosol nucleation. *Nature* **2011**, *476*, 429–433. [CrossRef] [PubMed]
12. Cai, R.; Yin, R.; Li, X.; Xie, H.B.; Yang, D.; Kerminen, V.M.; Smith, J.N.; Ma, Y.; Hao, J.; Chen, J.; et al. Significant contributions of trimethylamine to sulfuric acid nucleation in polluted environments. *npj Clim. Atmos. Sci.* **2023**, *6*, 75. [CrossRef]
13. Bianchi, F.; Kurtén, T.; Riva, M.; Mohr, C.; Rissanen, M.P.; Roldin, P.; Berndt, T.; Crounse, J.D.; Wennberg, P.O.; Mentel, T.F.; et al. Highly oxygenated organic molecules (HOM) from gas-phase autoxidation involving peroxy radicals: A key contributor to atmospheric aerosol. *Chem. Rev.* **2019**, *119*, 3472–3509. [CrossRef] [PubMed]
14. Nie, W.; Yan, C.; Yang, L.; Roldin, P.; Liu, Y.; Vogel, A.L.; Molteni, U.; Stolzenburg, D.; Finkenzeller, H.; Amorim, A.; et al. NO at low concentration can enhance the formation of highly oxygenated biogenic molecules in the atmosphere. *Nat. Commun.* **2023**, *14*, 3347. [CrossRef] [PubMed]
15. Brean, J.; Harrison, R.M.; Shi, Z.; Beddows, D.C.S.; Acton, W.J.F.; Hewitt, C.N.; Squires, F.A.; Lee, J. Observations of highly oxidized molecules and particle nucleation in the atmosphere of Beijing. *Atmos. Chem. Phys.* **2019**, *19*, 14933–14947. [CrossRef]
16. Rose, C.; Zha, Q.; Dada, L.; Yan, C.; Lehtipalo, K.; Junninen, H.; Mazon, S.B.; Jokinen, T.; Sarnela, N.; Sipilä, M.; et al. Observations of biogenic ion-induced cluster formation in the atmosphere. *Sci. Adv.* **2018**, *4*, eaar5218. [CrossRef]

17. Yan, C.; Nie, W.; Vogel, A.L.; Dada, L.; Lehtipalo, K.; Stolzenburg, D.; Wagner, R.; Rissanen, M.P.; Xiao, M.; Ahonen, L.; et al. Size-dependent influence of NO_x on the growth rates of organic aerosol particles. *Sci. Adv.* **2020**, *6*, eaay4945. [CrossRef]
18. Kirkby, J.; Amorim, A.; Baltensperger, U.; Carslaw, K.S.; Christoudias, T.; Curtius, J.; Donahue, N.M.; Haddad, I.E.; Flagan, R.C.; Gordon, H.; et al. Atmospheric new particle formation from the CERN CLOUD experiment. *Nat. Geosci.* **2023**, *16*, 948–957. [CrossRef]
19. Guo, Y.; Yan, C.; Liu, Y.; Qiao, X.; Zheng, F.; Zhang, Y.; Zhou, Y.; Li, C.; Fan, X.; Lin, Z.; et al. Seasonal variation in oxygenated organic molecules in urban Beijing and their contribution to secondary organic aerosol. *Atmos. Chem. Phys.* **2022**, *22*, 10077–10097. [CrossRef]
20. Liu, Y.; Nie, W.; Li, Y.; Ge, D.; Liu, C.; Xu, Z.; Chen, L.; Wang, T.; Wang, L.; Sun, P.; et al. Formation of condensable organic vapors from anthropogenic and biogenic volatile organic compounds (VOCs) is strongly perturbed by NO_x in eastern China. *Atmos. Chem. Phys.* **2021**, *21*, 14789–14814. [CrossRef]
21. Cheng, X.; Li, Y.J.; Zheng, Y.; Liao, K.; Koenig, T.K.; Ge, Y.; Zhu, T.; Ye, C.; Qiu, X.; Chen, Q. Oxygenated organic molecules produced by low-NO_x photooxidation of aromatic compounds: Contributions to secondary organic aerosol and steric hindrance. *Atmos. Chem. Phys.* **2024**, *24*, 2099–2112. [CrossRef]
22. Zheng, P.; Chen, Y.; Wang, Z.; Liu, Y.; Pu, W.; Yu, C.; Xia, M.; Xu, Y.; Guo, J.; Guo, Y.; et al. Molecular characterization of oxygenated organic molecules and their dominating roles in particle growth in Hong Kong. *Environ. Sci. Technol.* **2023**, *57*, 7764–7776. [CrossRef]
23. Zhang, H.; Wang, W.; Fan, L.; Li, J.; Ren, Y.; Li, H.; Gao, R.; Xu, Y. The role of sulfur cycle in new particle formation: Cycloaddition reaction of SO_3 to H_2S. *J. Environ. Sci.* **2025**, *148*, 489–501. [CrossRef]
24. Wennberg, P.O.; Bates, K.H.; Crounse, J.D.; Dodson, L.G.; McVay, R.C.; Mertens, L.A.; Nguyen, T.B.; Praske, E.; Schwantes, R.H.; Smarte, M.D.; et al. Gas-phase reactions of isoprene and its major oxidation products. *Chem. Rev.* **2018**, *118*, 3337–3390. [CrossRef]
25. Ning, A.; Zhong, J.; Li, L.; Li, H.; Liu, J.; Liu, L.; Liang, Y.; Li, J.; Zhang, X.; Francisco, J.S.; et al. Chemical implications of rapid reactive absorption of I_2O_4 at the air-water interface. *J. Am. Chem. Soc.* **2023**, *145*, 10817–10825. [CrossRef]
26. Zhang, H.; Gao, R.; Li, H.; Li, Y.; Xu, Y.; Chai, F. Formation mechanism of typical aromatic sulfuric anhydrides and their potential role in atmospheric nucleation process. *J. Environ. Sci.* **2023**, *123*, 54–64. [CrossRef]
27. Ning, A.; Liu, L.; Zhang, S.; Yu, F.; Du, L.; Ge, M.; Zhang, X. The critical role of dimethylamine in the rapid formation of iodic acid particles in marine areas. *npj Clim. Atmos. Sci.* **2022**, *5*, 92. [CrossRef]
28. Li, J.; Wu, N.; Chu, B.; Ning, A.; Zhang, X. Molecular-level study on the role of methanesulfonic acid in iodine oxoacid nucleation. *Atmos. Chem. Phys.* **2024**, *24*, 3989–4000. [CrossRef]
29. Nie, W.; Yan, C.; Huang, D.D.; Wang, Z.; Liu, Y.; Qiao, X.; Guo, Y.; Tian, L.; Zheng, P.; Xu, Z.; et al. Secondary organic aerosol formed by condensing anthropogenic vapours over China's megacities. *Nat. Geosci.* **2022**, *15*, 255–261. [CrossRef]
30. Wang, M.; Chen, D.; Xiao, M.; Ye, Q.; Stolzenburg, D.; Hofbauer, V.; Ye, P.; Vogel, A.L.; Mauldin, R.L., III; Amorim, A.; et al. Photo-oxidation of aromatic hydrocarbons produces low-volatility organic compounds. *Environ. Sci. Technol.* **2020**, *54*, 7911–7921. [CrossRef]
31. Grimme, S. Do special noncovalent π–π stacking interactions really exist? *Angew. Chem. Int. Ed.* **2008**, *47*, 3430–3434. [CrossRef] [PubMed]
32. Ji, S.; Guo, Y.; Yan, W.; Wei, F.; Ding, J.; Hong, W.; Wu, X.; Ku, T.; Yue, H.; Sang, N. $PM_{2.5}$ exposure contributes to anxiety and depression-like behaviors via phenyl-containing compounds interfering with dopamine receptor. *Proc. Natl. Acad. Sci. USA* **2024**, *121*, e2319595121. [CrossRef]
33. Strollo, C.M.; Ziemann, P.J. Investigation of the formation of benzoyl peroxide, benzoic anhydride, and other potential aerosol products from gas–phase reactions of benzoylperoxy radicals. *Atmos. Environ.* **2016**, *130*, 202–210. [CrossRef]
34. Ji, Y.; Zhao, J.; Terazono, H.; Misawa, K.; Levitt, N.P.; Li, Y.; Lin, Y.; Peng, J.; Wang, Y.; Duan, L.; et al. Reassessing the atmospheric oxidation mechanism of toluene. *Proc. Natl. Acad. Sci. USA* **2017**, *114*, 8169–8174. [CrossRef]
35. Nishino, N.; Arey, J.; Atkinson, R. 2-formylcinnamaldehyde formation yield from the OH radical-initiated reaction of naphthalene: Effect of NO_2 concentration. *Environ. Sci. Technol.* **2012**, *46*, 8198–8204. [CrossRef] [PubMed]
36. Li, D.; Huang, W.; Wang, D.; Wang, M.; Thornton, J.A.; Caudillo, L.; Rörup, B.; Marten, R.; Scholz, W.; Finkenzeller, H.; et al. Nitrate radicals suppress biogenic new particle formation from monoterpene oxidation. *Environ. Sci. Technol.* **2024**, *58*, 1601–1614. [CrossRef]
37. Mehra, A.; Wang, Y.; Krechmer, J.E.; Lambe, A.; Majluf, F.; Morris, M.A.; Priestley, M.; Bannan, T.J.; Bryant, D.J.; Pereira, K.L.; et al. Evaluation of the chemical composition of gas- and particle-phase products of aromatic oxidation. *Atmos. Chem. Phys.* **2020**, *20*, 9783–9803. [CrossRef]
38. Wang, Y.; Mehra, A.; Krechmer, J.E.; Yang, G.; Hu, X.; Lu, Y.; Lambe, A.; Canagaratna, M.; Chen, J.; Worsnop, D.; et al. Oxygenated products formed from OH-initiated reactions of trimethylbenzene: Autoxidation and accretion. *Atmos. Chem. Phys.* **2020**, *20*, 9563–9579. [CrossRef]

39. Wang, S.; Zhang, Q.; Wang, W.; Wang, Q. Unexpected enhancement of sulfuric acid-driven new particle formation by alcoholic amines: The role of ion-induced nucleation. *J. Environ. Manag.* **2023**, *347*, 119079. [CrossRef] [PubMed]
40. Shi, X.; Huang, G.; Yang, D.; Zhang, Q.; Zong, W.; Cheng, J.; Sui, X.; Yuan, F.; Wang, W. Theoretical study of the formation and nucleation mechanism of highly oxygenated multi-functional organic compounds produced by α-pinene. *Sci. Total Environ.* **2021**, *780*, 146422. [CrossRef]
41. Ma, F.; Xie, H.B.; Zhang, R.; Su, L.; Jiang, Q.; Tang, W.; Chen, J.; Engsvang, M.; Elm, J.; He, X.C. Enhancement of atmospheric nucleation precursors on iodic acid-induced nucleation: Predictive model and mechanism. *Environ. Sci. Technol.* **2023**, *57*, 6944–6954. [CrossRef]
42. Zhang, R.; Xie, H.B.; Ma, F.; Chen, J.; Iyer, S.; Simon, M.; Heinritzi, M.; Shen, J.; Tham, Y.J.; Kurtén, T.; et al. Critical role of iodous acid in neutral iodine oxoacid nucleation. *Environ. Sci. Technol.* **2022**, *56*, 14166–14177. [CrossRef]
43. Elm, J.; Ayoubi, D.; Engsvang, M.; Jensen, A.B.; Knattrup, Y.; Kubečka, J.; Bready, C.J.; Fowler, V.R.; Harold, S.E.; Longsworth, O.M.; et al. Quantum chemical modeling of organic enhanced atmospheric nucleation: A critical review. *WIREs Comput. Mol. Sci.* **2023**, *13*, e1662. [CrossRef]
44. Lian, Y.; Bai, X.; Yuan, R.; Wei, T.; Mao, H.; Peng, J.; Jiang, S. Atmospheric aerosol nucleation: A methodological review of theoretical calculations and molecular simulation. *Environ. Sci. Atmos.* 2026, *Advance Article*. [CrossRef]
45. Neese, F. The ORCA program system. *WIREs Comput. Mol. Sci.* **2012**, *2*, 73–78. [CrossRef]
46. Elm, J.; Kubečka, J.; Besel, V.; Jääskeläinen, M.J.; Halonen, R.; Kurtén, T.; Vehkamäki, H. Modeling the formation and growth of atmospheric molecular clusters: A review. *J. Aerosol Sci.* **2020**, *149*, 105621. [CrossRef]
47. Frisch, M.J.; Trucks, G.W.; Schlegel, H.B.; Scuseria, G.E.; Robb, M.A.; Cheeseman, J.R.; Scalmani, G.; Barone, V.; Petersson, G.A.; Nakatsuji, H.; et al. *Gaussian 16*, Revision A.03; Gaussian, Inc.: Wallingford, CT, USA, 2016.
48. Liu, Z.; Lu, T.; Chen, Q. Intermolecular interaction characteristics of the all-carboatomic ring, cyclo[18]carbon: Focusing on molecular adsorption and stacking. *Carbon* **2021**, *171*, 514–523. [CrossRef]
49. Wang, H.; Zhao, X.; Zuo, C.; Ma, X.; Xu, F.; Sun, Y.; Zhang, Q. A molecular understanding of the interaction of typical aromatic acids with common aerosol nucleation precursors and their atmospheric implications. *RSC Adv.* **2019**, *9*, 36171–36181. [CrossRef] [PubMed]
50. Bandow, H.; Washida, N.; Akimoto, H. Ring-cleavage reactions of aromatic hydrocarbons studied by FT–IR Spectroscopy. I. Photooxidation of toluene and benzene in the NO_x–air system. *Bull. Chem. Soc. Jpn.* **2006**, *58*, 2531–2540. [CrossRef]
51. Dong, Z.; Tang, R.; Liu, H.; Zhang, Q.; Zong, W.; Cheng, J.; Shi, X. The formation mechanism of highly oxygenated organic molecules produced by toluene in the urban atmosphere. *Atmos. Environ.* **2023**, *295*, 119555. [CrossRef]
52. Riva, M.; Healy, R.M.; Flaud, P.-M.; Perraudin, E.; Wenger, J.C.; Villenave, E. Kinetics of the gas-phase reactions of chlorine atoms with naphthalene, acenaphthene, and acenaphthylene. *J. Phys. Chem. A* **2014**, *118*, 3535–3540. [CrossRef]
53. Zhang, R.; Khalizov, A.; Wang, L.; Hu, M.; Xu, W. Nucleation and growth of nanoparticles in the atmosphere. *Chem. Rev.* **2012**, *112*, 1957–2011. [CrossRef]
54. Chen, M.; Titcombe, M.; Jiang, J.; Jen, C.; Kuang, C.; Fischer, M.L.; Eisele, F.L.; Siepmann, J.I.; Hanson, D.R.; Zhao, J.; et al. Acid–base chemical reaction model for nucleation rates in the polluted atmospheric boundary layer. *Proc. Natl. Acad. Sci. USA* **2012**, *109*, 18713–18718. [CrossRef]
55. Bianchi, F.; Tröstl, J.; Junninen, H.; Frege, C.; Henne, S.; Hoyle, C.R.; Molteni, U.; Herrmann, E.; Adamov, A.; Bukowiecki, N.; et al. New particle formation in the free troposphere: A question of chemistry and timing. *Science* **2016**, *352*, 1109–1112. [CrossRef]
56. Zhang, R.; Ma, F.; Zhang, Y.; Chen, J.; Elm, J.; He, X.C.; Xie, H.B. HIO_3–HIO_2-driven three-component nucleation: Screening model and cluster formation mechanism. *Environ. Sci. Technol.* **2024**, *58*, 649–659. [CrossRef]
57. Cai, R.; Yan, C.; Yang, D.; Yin, R.; Lu, Y.; Deng, C.; Fu, Y.; Ruan, J.; Li, X.; Kontkanen, J.; et al. Sulfuric acid–amine nucleation in urban Beijing. *Atmos. Chem. Phys.* **2021**, *21*, 2457–2468. [CrossRef]
58. Myllys, N.; Chee, S.; Olenius, T.; Lawler, M.; Smith, J. Molecular-level understanding of synergistic effects in sulfuric acid–amine–ammonia mixed clusters. *J. Phys. Chem. A* **2019**, *123*, 2420–2425. [CrossRef] [PubMed]
59. Roman, C.; Arsene, C.; Bejan, I.G.; Olariu, R.I. Investigations into the gas-phase photolysis and OH radical kinetics of nitrocatechols: Implications of intramolecular interactions on their atmospheric behaviour. *Atmos. Chem. Phys.* **2022**, *22*, 2203–2219. [CrossRef]
60. Jenkin, M.E.; Valorso, R.; Aumont, B.; Rickard, A.R.; Wallington, T.J. Estimation of rate coefficients and branching ratios for gas-phase reactions of OH with aromatic organic compounds for use in automated mechanism construction. *Atmos. Chem. Phys.* **2018**, *18*, 9329–9349. [CrossRef]
61. Zhang, Q.; Xu, Y.; Jia, L. Secondary organic aerosol formation from OH-initiated oxidation of m-xylene: Effects of relative humidity on yield and chemical composition. *Atmos. Chem. Phys.* **2019**, *19*, 15007–15021. [CrossRef]
62. Zhang, H.; Wang, J.; Dong, B.; Xu, F.; Liu, H.; Zhang, Q.; Zong, W.; Shi, X. New mechanism for the participation of aromatic oxidation products in atmospheric nucleation. *Sci. Total Environ.* **2024**, *917*, 170487. [CrossRef]

63. Riva, M.; Healy, R.M.; Flaud, P.M.; Perraudin, E.; Wenger, J.C.; Villenave, E. Gas- and particle-phase products from the photooxidation of acenaphthene and acenaphthylene by OH radicals. *Atmos. Environ.* **2017**, *151*, 34–44. [CrossRef]
64. Zeng, M.; Liao, Z.; Wang, L. Atmospheric oxidation of gaseous anthracene and phenanthrene initiated by OH radicals. *Atmos. Environ.* **2020**, *234*, 117587. [CrossRef]
65. Runberg, H.L.; Majestic, B.J. Hydroxyl radical (OH) formation during the photooxidation of anthracene and its oxidized derivatives. *Atmos. Environ.* **2022**, *286*, 119214. [CrossRef]
66. Quéléver, L.L.J.; Kristensen, K.; Normann Jensen, L.; Rosati, B.; Teiwes, R.; Daellenbach, K.R.; Peräkylä, O.; Roldin, P.; Bossi, R.; Pedersen, H.B.; et al. Effect of temperature on the formation of highly oxygenated organic molecules (HOMs) from alpha-pinene ozonolysis. *Atmos. Chem. Phys.* **2019**, *19*, 7609–7625. [CrossRef]
67. Dada, L.; Stolzenburg, D.; Simon, M.; Fischer, L.; Heinritzi, M.; Wang, M.; Xiao, M.; Vogel, A.L.; Ahonen, L.; Amorim, A.; et al. Role of sesquiterpenes in biogenic new particle formation. *Sci. Adv.* **2023**, *9*, adi5297. [CrossRef]
68. Kristensen, K.; Enggrob, K.L.; King, S.M.; Worton, D.R.; Platt, S.M.; Mortensen, R.; Rosenoern, T.; Surratt, J.D.; Bilde, M.; Goldstein, A.H.; et al. Formation and occurrence of dimer esters of pinene oxidation products in atmospheric aerosols. *Atmos. Chem. Phys.* **2013**, *13*, 3763–3776. [CrossRef]
69. Molteni, U.; Bianchi, F.; Klein, F.; El Haddad, I.; Frege, C.; Rossi, M.J.; Dommen, J.; Baltensperger, U. Formation of highly oxygenated organic molecules from aromatic compounds. *Atmos. Chem. Phys.* **2018**, *18*, 1909–1921. [CrossRef]
70. Zaytsev, A.; Koss, A.R.; Breitenlechner, M.; Krechmer, J.E.; Nihill, K.J.; Lim, C.Y.; Rowe, J.C.; Cox, J.L.; Moss, J.; Roscioli, J.R.; et al. Mechanistic study of the formation of ring-retaining and ring-opening products from the oxidation of aromatic compounds under urban atmospheric conditions. *Atmos. Chem. Phys.* **2019**, *19*, 15117–15129. [CrossRef]
71. Yin, R.; Yan, C.; Cai, R.; Li, X.; Shen, J.; Lu, Y.; Schobesberger, S.; Fu, Y.; Deng, C.; Wang, L.; et al. Acid–base clusters during atmospheric new particle formation in urban Beijing. *Environ. Sci. Technol.* **2021**, *55*, 10994–11005. [CrossRef] [PubMed]
72. Shen, J.; Elm, J.; Xie, H.B.; Chen, J.; Niu, J.; Vehkamäki, H. Structural effects of amines in enhancing methanesulfonic acid-driven new particle formation. *Environ. Sci. Technol.* **2020**, *54*, 13498–13508. [CrossRef] [PubMed]
73. Shen, J.; Xie, H.B.; Elm, J.; Ma, F.; Chen, J.; Vehkamäki, H. Methanesulfonic acid-driven new particle formation enhanced by monoethanolamine: A computational study. *Environ. Sci. Technol.* **2019**, *53*, 14387–14397. [CrossRef] [PubMed]
74. Zhang, X.; Lian, Y.; Tan, S.; Yin, S. Organosulfate produced from consumption of SO_3 speeds up sulfuric acid–dimethylamine atmospheric nucleation. *Atmos. Chem. Phys.* **2024**, *24*, 3593–3612. [CrossRef]

Disclaimer/Publisher's Note: The statements, opinions and data contained in all publications are solely those of the individual author(s) and contributor(s) and not of MDPI and/or the editor(s). MDPI and/or the editor(s) disclaim responsibility for any injury to people or property resulting from any ideas, methods, instructions or products referred to in the content.